Atomistic insights into cardiolipin binding sites of cytochrome c oxidase

Malkamäki, Aapo Erkki Matias

2019-03-01

Malkamäki , A E M & Sharma , V 2019 , ' Atomistic insights into cardiolipin binding sites of cytochrome c oxidase ' , Biochimica et Biophysica Acta. Bioenergetics , vol. 1860 , no. 3 , pp. 224-232 . https://doi.org/10.1016/j.bbabio.2018.11.004

http://hdl.handle.net/10138/298527
https://doi.org/10.1016/j.bbabio.2018.11.004

BBA - Bioenergetics 1860 (2019) 224–232

Contents lists available at ScienceDirect

BBA - Bioenergetics

journal homepage: www.elsevier.com/locate/bbabio

Atomistic insights into cardiolipin binding sites of cytochrome *c* oxidase

Aapo Malkamäki[a], Vivek Sharma[a,b,*]

[a] Department of Physics, P. O. Box 64, University of Helsinki, Helsinki 00014, Finland
[b] Institute of Biotechnology, P. O. Box 56, University of Helsinki, Helsinki 00014, Finland

ARTICLE INFO

Keywords:
Molecular dynamics simulations
Lipid-protein interactions
Proton pumping
Energy transduction

ABSTRACT

Mitochondrial cytochrome *c* oxidase couples the reduction of oxygen to proton pumping. Despite an overall good understanding of its molecular mechanism, the role of cardiolipin in protein function is not understood. Here, we have studied the cardiolipin-protein interactions in a dynamic context by means of atomistic molecular dynamics simulations performed on the entire structure of monomeric and dimeric forms of the enzyme. Several microseconds of simulation data reveal that the crystallographic cardiolipin molecules that *glue* two monomers together bind weakly in hybrid and single-component lipid bilayers and dissociate rapidly. Atomistic simulations performed in the absence of tightly bound cardiolipin molecules strongly perturb the structural integrity of subunits III and VIIa, thereby highlighting an indispensable nature of lipid-protein interactions in enzyme function such as proton uptake and oxygen channeling. Our results demonstrate the strength of molecular simulations in providing direct atomic description of lipid-protein processes that are difficult to achieve experimentally.

1. Introduction

The electron transport chains of mitochondria and bacteria terminate in heme-copper oxidases, which catalyze the four-electron reduction of molecular oxygen (O_2) to water (H_2O) and conserve the free energy by pumping protons across the membrane [1,2]. The superfamily of heme-copper oxidases is divided into three subclasses, A-, B- and C-type [3]. Among these, the A-type oxidases are most studied, and their mechanism of redox-coupled proton pumping is relatively well-understood [1,2]. In mammalian mitochondria, the A-type oxidases are cytochrome *c* oxidases (CcOs), because water soluble protein cytochrome *c* donates the electrons to the active site via Cu_A/heme *a* (see Fig. 1, [4]). All heme-copper oxidases are characterized by a unique active site in which a high-spin heme is magnetically coupled with a Cu ion ligated by two histidines and one covalently linked histidine-tyrosine system (Fig. 1B). The tyrosine (Tyr244 in bovine enzyme) is a structurally conserved feature in CcOs, located in helix VI or VII of the A-/B- or C-type oxidases, respectively [5].

The oxygen diffuses in from the lipid membrane and is fully reduced to water by transfer of four electrons and four protons at the buried active site (Fig. 1B). The oxygen reduction reaction is tightly coupled to proton pumping. To transfer protons from the N-side to the P-side or to the site of oxygen reduction, hydrated cavities and titratable amino acid residues play an important role (Fig. 1A). Such proton transfer pathways have been characterized in the A-type oxidases by structural, biochemical and computational methods (Fig. 1A) [1,2,6].

Many mechanistic aspects of redox-coupled proton pumping are well-understood, while subtle issues are being explored by means of multi-scale computational techniques [7–10]. However, roles of lipids in enzyme function remain unclear. Such aspects are especially important because mammalian CcO tightly binds cardiolipin (CL) molecules, some of which have been resolved crystallographically and characterized with mass spectrometric analysis (Fig. 2) in spectacular work by Yoshikawa and colleagues [11]. Yet, their functions remain unclear in the context of enzyme mechanism or regulation.

Cardiolipins are unique lipids which have a highly charged but small head group, and four hydrocarbon tails. They are primarily found in mitochondrial membranes, where all four tails are of linoleoyl nature [12,13]. Interestingly, atomic three dimensional structures of all respiratory complexes reveal CL binding sites [14]. In the case of bovine CcO, which is crystallized in its dimeric form [11], four CL molecules are observed (two per monomer) (Fig. 2). In partial agreement with the structural data, purified and detergent solubilized *monomeric* CcO binds 3–4 CL molecules (two tightly bound and 1–2 loosely bound) [15,16]. However, the binding locations and their specific roles in enzyme function remain unclear.

Abbreviations: CcO, cytochrome *c* oxidase; CL, cardiolipin; TGL, triglyceride; PC, phosphatidylcholine; PE, phosphatidylethanolamine; PG, phosphatidylglycerol

* Corresponding author at: Department of Physics, P. O. Box 64, University of Helsinki, 00014 Helsinki, Finland.
E-mail address: vivek.sharma@helsinki.fi (V. Sharma).

https://doi.org/10.1016/j.bbabio.2018.11.004
Received 6 August 2018; Received in revised form 21 September 2018; Accepted 7 November 2018
Available online 08 November 2018

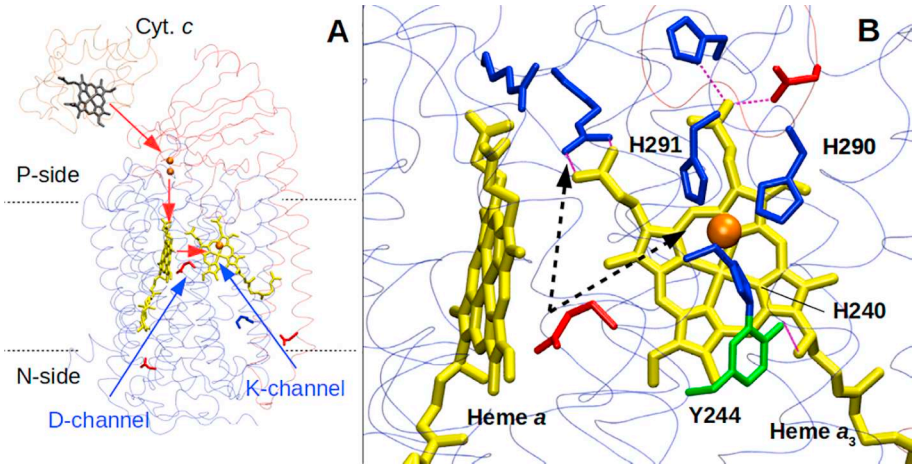

Fig. 1. (A) A Cyt *c*- C*c*O complex (PDB 5IY5). The two membrane-bound catalytic subunits of C*c*O are shown in blue (subunit I) and red (subunit II) ribbons, whereas orange scaffold shows the electron donor cyt *c*. Proton channels (D and K channel) translocate protons from the N-side of the membrane to the active site (shown as blue arrows). The electron transfer path is marked with red arrows (cyt *c* → Cu_A → heme *a* → active site). Hemes *a* and a_3 (yellow), coppers (bimetallic Cu_A and Cu_B in orange), and acidic, basic and polar amino acids in proton channels are shown in red, blue and green, respectively. (B) Zoomed-in view of the active site of C*c*O. Low spin (left) and high spin (right) hemes are shown together with Cu_B, the site where oxygen binds and is reduced. Dashed arrows show putative paths of protons towards the P-side of the membrane and towards the site of oxygen reduction.

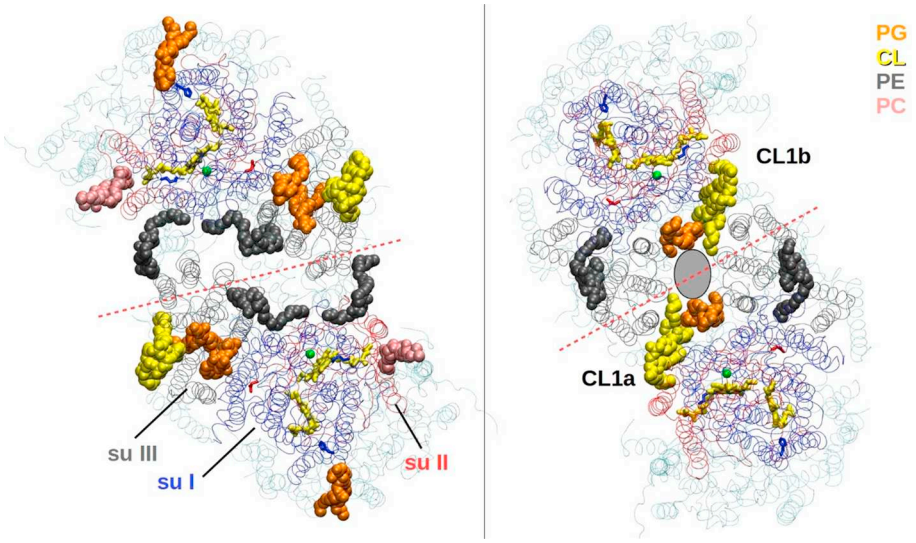

Fig. 2. Crystallographically resolved lipids in the crystal structure of C*c*O (PDB 2DYR). Left and right are views from the mitochondrial matrix and inter membrane space (IMS), respectively. The red dotted line shows separation between two monomers, and grey area highlights an empty region between the dimers (see main text). Hemes (yellow licorice representation), copper (green), and some of the charged and polar residues that belong to proton channels are also shown. Bound lipid molecules are shown in van der Waals representation. Subunits (su) I, II and III are in blue, red and grey ribbons, respectively.

It is well-known that delipidation of C*c*O by means of strong agents that also remove tightly bound CLs perturbs the activity of the enzyme (ca. 50% decrease) [16], but molecular mechanism by which it occurs is not known. In contrast, removal of other lipids (such as PC or PE) has a mild effect on the activity. A number of pioneering studies from the Robinson group revealed that phospholipids affect the stability of the enzyme [17], and bovine C*c*O subunits VIa, VIb, III and VIIa are the first ones to dissociate upon variety of chemical treatments [18]. However, how lipids, especially CLs, provide stability to protein subunits is not understood.

The dimeric bovine C*c*O structure reveals a number of crystallographically resolved lipids, out of which 4 are CL, and others are phosphatidylcholine/PC (2), phosphatidylethanolamine/PE (6) and phosphatidylglycerol/PG (6). In each monomer, a CL molecule is found next to subunit III (chains C and P) with its head group pointing towards the N side of the membrane (mitochondrial matrix) (left, Fig. 2). A second buried CL with its head group towards the P side of the membrane is observed next to subunits III and VIa, together with another interface provided by subunits I and II of another monomer, suggesting its role in *gluing* the two monomers together (right, Fig. 2). In addition, the highly conserved V-shaped subunit III houses three lipids (2 PG and 1 PE in bovine enzyme), which are deeply buried in contrast to other lipids bound on protein surface (Fig. 2).

The structural data on oxidase provide exquisite details of the lipid binding sites, and in particular how CL molecules bind. However, *dynamical* aspects of lipid-protein interactions are entirely missing, which are necessary to understand their role in enzyme function. In this work, we have performed atomistic classical molecular dynamics (MD) simulations of dimeric and monomeric forms of bovine C*c*O (totaling ~18 μs). To the best of our knowledge, simulations of these lengths and dimensions have not been performed earlier and provide entirely new dynamic insights into the two crystallographic CL binding sites of oxidase. The simulations show that, although most of the crystallographically observed lipids remain bound to the protein, the CL molecules that are located between the two monomers bind weakly. Providing microscopic insights to the biochemical data for the first time, we also show that by stripping enzyme of its tightly bound CL molecules, the structure and stability are strongly perturbed, which inevitably would lead to activity loss.

2. Computational methods

2.1. Model systems

Fully atomistic models of dimeric (D) and monomeric (M) forms of C*c*O from *Bos taurus* (PDB: 2DYR) were constructed to perform classical molecular dynamics (MD) simulations. The systems were modeled with or without crystallographically resolved lipids (and detergent molecules). The crystallographic water molecules and ions were included in all simulation setups. See Table 1 for systems constructed in this work. CHARMM-GUI [19] was used to construct the membrane-protein system, in which hybrid lipid bilayer mimicking the inner

Table 1
Model systems and simulation lengths.

Setup	Monomer (M)/Dimer (D)	Crystallographic lipids	Lipid bilayer[a]	Simulation lengths ~ (μs)
1	D	No	Mixed *u*: 181 PC + 115 PE + 72 CL *l*: 180 PC + 108 PE + 72 CL	3.0
2	D	Yes	Mixed *u*: 181 PC + 115 PE + 72 CL *l*: 180 PC + 108 PE + 72 CL	3.3
3	M	No	Mixed *u*: 91 PC + 57 PE + 36 CL *l*: 90 PC + 54 PE + 36 CL	2.2
4	M	Yes	Mixed *u*: 91 PC + 57 PE + 36 CL *l*: 90 PC + 54 PE + 36 CL	2.1
5	M	No	Mixed *u*: 91 PC + 57 PE + 36 CL *l*: 90 PC + 54 PE + 36 CL CL modeled close to the protein surface	2.1
6	M	No	Mixed *u*: 91 PC + 57 PE + 36 CL *l*: 90 PC + 54 PE + 36 CL CL modeled far away from the protein surface	2.4
7	M	Yes (all TGL molecules replaced by CL)	Only PC *u*: 218 *l*: 212	1.0
8	M	No (only PG/PE molecules bound to su III are included)	Only PC *u*: 218 *l*: 212	2.0

[a] *u* and *l* denote the upper (P side) and lower (N side) leaflets of the membrane, respectively.

mitochondrial membrane was used. The multi component lipid bilayer consisted of three types of lipids; charge neutral POPC (1-Palmitoyl-2-oleoyl-sn-glycero-3-phosphocholine), charge neutral POPE (1-Palmitoyl-2-oleoyl-sn-glycero-3-phosphoenthanolamine) and dianionic CL (tetra linoleoyl cardiolipin), which were in a ratio of 5:3:2. A model system with single component POPC lipid bilayer was also constructed (see Table 1 and Fig. S1). The solvent water molecules (~128,000 in dimeric systems and ~65,000 in monomeric systems) were added together with the Na and Cl ions to neutralize the system and to achieve salt concentration of 150 mM. The dimeric systems had ~650 Na ions and 361 Cl ions, whereas monomeric systems had ~180 Cl ions together with 320 and 190 Na ions in with and without cardiolipin systems, respectively. Since there is an empty crevice in the middle of the two monomers, we modeled 7 lipids based on earlier suggestions [20], and to prevent it from getting unnaturally hydrated. The total system size was ~280,000 and ~550,000 atoms in monomeric and dimeric models, respectively.

CcO contains redox active components, and therefore, we used force field parameterization by Johansson et al. [21] and modeled all metals in their oxidized state. The active site structure in CcO comprises a high spin heme and a Cu_B center, and in all simulations the high spin heme was ligated by a water molecule, and Cu_B with a hydroxyl together with the highly conserved cross-linked tyrosine modeled anionic in nature [1]. All amino acids were considered in their standard protonation states, except Glu242, Lys319 and Asp364 of subunit I, which were kept neutral [22]. The N- and C-terminal were patched with CHARMM NTER and CTER patches, respectively, whereas only in case of chains G and T (subunit VIa), the termini were patched neutral due to the presence of N-terminal segment in the middle of the membrane in the crystal structure. The protein, membrane, water and ions were treated with the CHARMM force field [23–25].

2.2. Molecular dynamics simulations

The constructed systems were subjected to an energy minimization ($2 \times 50{,}000$ steps with max force $< 1000\,kJ\,mol^{-1}\,nm^{-1}$), followed by a short equilibration run. During equilibration Berendsen barostat [26] and Nose-Hoover [27,28] thermostat were used. All MD simulations were performed with GROMACS (version 5.0) software [29]. A time step of 2 fs was used by constraining all bonds associated with hydrogens by means of LINCS algorithm [30]. The temperature and pressure were kept constant by Nose-Hoover [27,28] thermostat and Parrinello-Rahman [31] barostat, respectively, during the production runs.

2.3. Simulation trajectory analysis

The root mean square deviation (RMSD) of protein reveals that the model systems are stable (Fig. S1). The simulation trajectory analysis was performed by VMD [32] and by in-house scripts. The lipid occupancy plots, CL unbinding events and CL binding sites are based on unbiased equilibrium MD simulations that are without any restraints or constraints. To identify key residues that interact with CLs, we first selected residues that were within 3 Å of CL molecules, which were differentiated based on their head groups, tails and their location in upper or lower leaflet of the membrane. From the obtained set of residues, those were picked that had at least half common interactions as the residue with strongest (longest) interaction with CL. Then the picked residues were removed from a pool (initially the full set) and a new strongest residue was selected from the pool. This was repeated until the pool was empty. The key residues are described in Tables 2, S1 and S2.

3. Results

3.1. Cardiolipin binding sites of bovine cytochrome c oxidase

Fully atomistic classical MD simulations of microseconds time scale were performed on the monomeric and dimeric forms of bovine cytochrome *c* oxidase in native-like lipid environment (Table 1 and Methods). The data from multiple independent simulations show that lipids, in particular dianionic CLs, bind to specific sites on the surface of the protein. The occupancy plots in Fig. 3 display the CL binding sites, which have been numbered from I–VIII, analogous to a previous coarse-grained (CG) simulation study [33]. We define a region on the protein surface to be a putative CL binding site if the occupancy at the site is ca. 40%, roughly double that of the bulk concentration. Figs. S2–S4 display the CL occupancy from setups 2–4, and figs. S5 and S6 by combining the

Table 2
Key residues that form charged, polar and hydrophobic interactions with the head group (H) and tails (T) of CL molecules at selected binding sites (I, IX and X) from setup 4. Subunits are identified by a superscript single letter chain name as in PDB 2DYR. Note CLs at CL1a/b (sites IX/X) are loosely bound.

Binding site (head group, H or tails, T)	Charged	Polar	Hydrophobic
I (H)	$R221^{C}$ $R59^{C}$ $K224^{C}$ $R63^{C}$	$Y55^{C}$	$V5^{J}$ $I62^{C}$ $F67^{C}$
IX (H)	$D300^{A}$	$Y85^{B}$	$V299^{A}$ $L81^{B}$ $A303^{A}$
X (H)	–	$H38^{G}$	$L37^{G}$
I (T)	$R59^{C}$	$T213^{C}$ $T27^{J}$ $T48^{C}$ $Y55^{C}$	$W58^{C}$ $I62^{C}$ $F220^{C}$ $M51^{C}$ $L52^{C}$ $I209^{C}$ $V217^{C}$ $I216^{C}$ $L31^{J}$
IX (T)		$Y304^{A}$ $S307^{A}$	$I74^{B}$ $L73^{B}$ $L283^{A}$ $A77^{B}$ $F282^{A}$ $I314^{A}$ $A70^{B}$ $I286^{A}$ $M310^{A}$ $L81^{B}$ $A303^{A}$ $I311^{A}$
X (T)		$S27^{G}$ $N34^{G}$	$L37^{G}$ $L131^{C}$ $L33^{G}$ $L30^{G}$

trajectory data of setups 1 and 2 (dimeric), and 3 and 4 (monomeric), respectively. The occupancy analyses reveal that CL populates the crystallographically observed CL binding site I (Fig. 1), which remains fully occupied in simulation setups 2 and 4 (Fig. S2 and S4). Due to limited time scale of atomistic simulations, multiple CL binding/unbinding events may not be observed within the time frame. Therefore, we performed additional simulations by modeling CL molecules proximal to the protein surface and far from it (setups 5 and 6, respectively) in order to enhance sampling statistics for the observed binding sites. The data from these simulations (Fig. S7 and S8) agree with the occupancy maps from setups 1–4, thereby providing statistical support to our findings.

3.2. Weak CL binding site at the monomer-monomer interface

The dimeric form of CcO is apparently stabilized by one or two CL molecules (CL1a/IX and CL1b/X, Fig. 2), which are tightly buried between the two monomers. Our simulations of the monomeric form (setup 4 in Table 1) reveal that these two lipids bind very weakly on the protein surface and dissociate within ca. 1 μs of simulation time (Fig. 4, panels A and B, and Supplementary video S1). A similar scenario is also observed when simulations are performed in a single component PC lipid bilayer (setup 7 in Table 1, Fig. 4, panels A and B). The remarkable departure of CL is initiated by the dissociation of head group shortly followed by its tails, suggesting somewhat tighter binding of lipid tails on hydrophobic protein surface, which is in strong contrast to the tighter binding of CL molecule at site I (Figs. 2 and 4) that is dominated by ionic interactions (see also Supplementary video S1). The data in Tables 2, S1 and S2 also clearly shows that the binding of CL1a/b lipids is predominantly non-polar in nature in contrast to site I CL, which is stabilized by charged-charged lipid-protein interactions.

Furthermore, in the simulations of monomeric and dimeric CcO performed without including the crystallographic lipids, no CL molecules bind to these sites in these time scales (Figs. 1 and S3), also when occupancy analysis is performed by combining the trajectories (Figs. S5 and S6). These data provide atomistic evidence for the weaker binding of CL molecules at these two sites. Our simulation data are also in agreement with the earlier proposals based on CG simulations [33] and biochemical analysis [34], and shows for the first time at an atomic level the mechanism of rapid unbinding of CL molecules.

We further analyzed if the removal of CL molecules buried between the two monomers affects the structure of the enzyme. Comparison of simulations with and without crystallographic lipids does not show any major differences in the dynamics of protein backbone. In fact, simulation setup 1 shows that the dimeric form is further stabilized due to formation of additional charged – charged interactions between the two monomers in comparison to the setup 2 (8.25 ± 2.23 in setup 1 versus 3.42 ± 1.65 in setup 2) (see also Fig. S9, panel A). Moreover, the interactions stabilize the interface between the subunits VIb (chains H and U in PDB 2DYR) (Fig. S10), which have been suggested to dissociate (together with VIa) upon removal of loosely bound CL [34]. Although simulation time scales are short to assess the long-time behaviour of dimeric CcO in the absence of bound CL, it appears that the removal of CL molecules buried between two monomers do not perturb the dimeric form of the enzyme in lipidic surroundings modeled here. However, destabilization of dimeric CcO in the absence of CL may still occur in detergent conditions. Indeed, it is known that protein oligomerization depends on membrane composition [35].

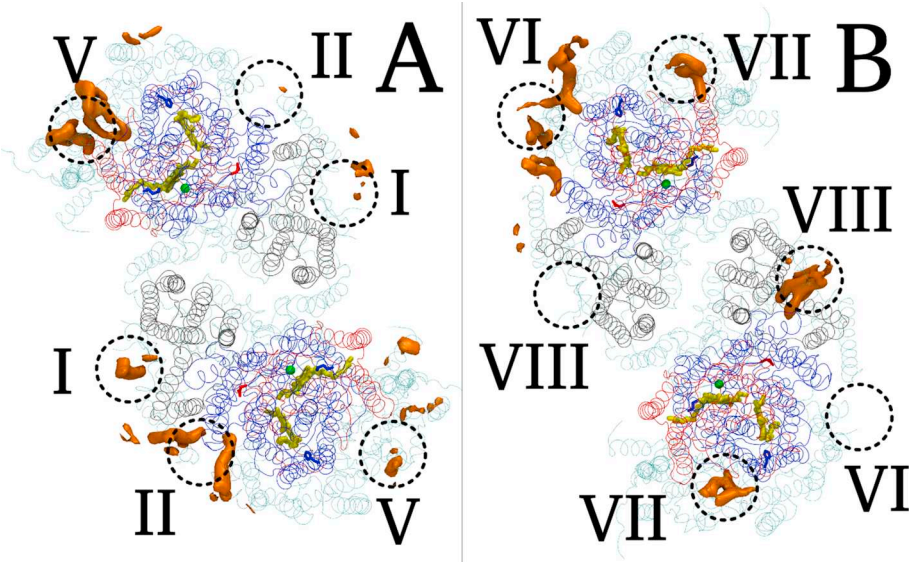

Fig. 3. CL occupancy map in brown (isosurface value of 0.4 or 40% occupancy) in the dimeric oxidase simulation setup 1, in which crystallographic lipidic components were not included. Views from the matrix side (A) and intermembrane space (B). Binding sites are marked with dotted circles and also labeled.

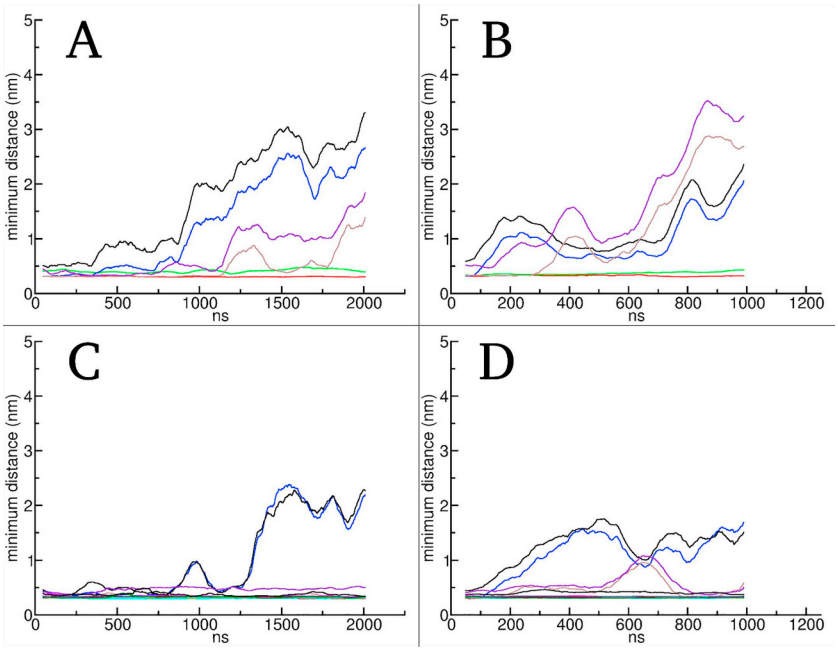

Fig. 4. Dissociation of CL1a (purple/brown traces) and CL1b (blue/black traces) from protein surface in monomeric simulations (A – setup 4, B – setup 7) shown as a minimum distance (in nm on y-axis) between protein Cα and whole head group or hydrophobic tail. The tightly bound CL at site I binds strongly (green/red traces in A and B). The dissociation of head group (black/purple/green) and tails (blue/brown/red) are shown separately. Panels C and D show the dissociation of PE molecules (found next to subunit VIa) in setups 4 and 7, respectively. In contrast, all PG lipids (and other PE lipids) remain tightly bound. The coloring for head groups and tails in panels C and D is same as in A and B. The data shown is a running average of 100 simulation snapshots with simulation time in ns on x-axis.

3.3. Tight CL binding site

In contrast to the weaker binding of CL molecules between the two monomers, the location next to subunit III (chain C) is a very high affinity CL binding site (site I). Its structure is well defined [11], and lipid-protein interactions at the site were studied by means of coarse-grained MD simulations [33]. However, due to missing atomistic details its role in enzyme mechanism remains entirely unknown [34]. Our simulations show that the site remains fully occupied for the entire simulation length (2–3 μs) (Fig. 4). This is due strong charge-charge interactions of CL with the protein (Tables 2, S1 and S2) that remain stable for microseconds. However, when simulations are performed by removing the tightly bound CL (setup 8), a remarkable disruption of protein architecture is observed in which a segment of subunit VIIa (chain J) unfolds, leading to a strong destabilization of tightly bound PG (and PE) lipid molecules in subunit III (Fig. 5 and Supplementary video S2). A further structural perturbation occurs in subunit III in which residues 225–235 that contain a stabilizing charged patch are displaced. This is in stark contrast to the data from other simulations with site I occupied (setups 2 and 4), which show stable lipid-protein arrangements in the region (Fig. 5D).

We suggest that stripping enzyme of tightly bound CL molecules lead to strong structural disruption, which causes loss of catalytic activity. The simulation data are also in excellent agreement with the experiments that the removal of all CL molecules results in protein structure destabilization leading to activity loss [16]. We emphasize that the direct observation of processes described here are not easily achieved by experiments, instead simulations of microsecond timescales, as performed here, are necessary to capture and display dynamic features to an atomic resolution.

3.4. Second tight CL binding site

Based on photolabeling studies, three to four different CL binding sites have been proposed, two of which are consistent with the crystal structure of bovine C*c*O (one tight binding site I, and another one gluing the two monomers – see above). However, experiments reveal that the third CL binding site (called site II here) resides somewhere in between the subunits VIIa and VIIc (also closer to subunit VIII) [34]. This position is occupied by a triglyceride molecule in the crystal structure of bovine oxidase. Our simulations (setups 2 and 4) show that in contrast to the rapid unbinding of crystallographic CL molecules on CL1a and CL1b sites, the hydrophobic triglyceride molecule remains bound to this site in these time scales (Fig. 6A) due to tight anchoring of its tails in the hydrophobic protein interior including interactions to the long farnesyl chain of heme *a*. In simulations, when crystallographic lipids and other

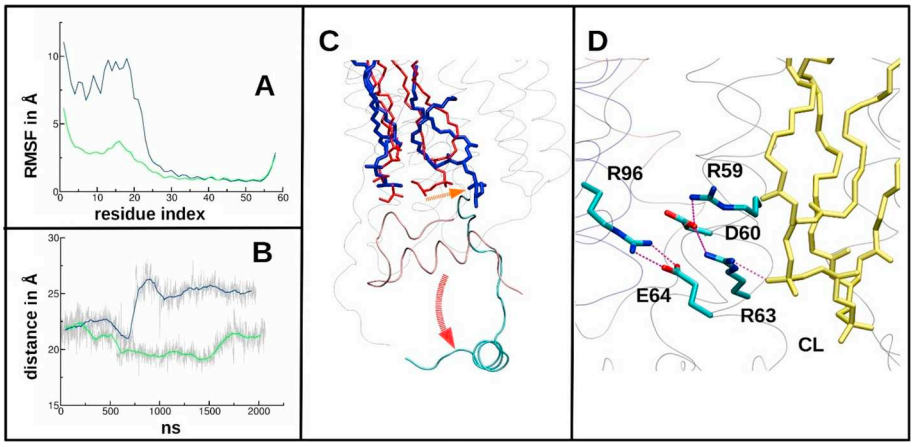

Fig. 5. A) Perturbation in the N-terminal segment of subunit VIIa due to the removal of site I CL as shown by higher root mean square fluctuation (RMSF) in blue (setup 8), whereas low RMSF of the same segment from simulation setup 4 is shown in green where CL is present. B) Displacement of tightly bound PG molecule in subunit III due to disturbed lipid-protein interactions (blue - setup 8, green – setup 4) as a distance from the proton uptake site Asp91 (see main text). C) Large scale conformational changes in the N-terminal segment of subunit VIIa upon removal of tightly bound CL at site 1 are shown by a red arrow. The orange arrow depicts the displacement of PG lipid from its tightly bound position (in red). D) Network of ionic interactions in subunits I and III with tightly bound site I CL molecule (yellow).

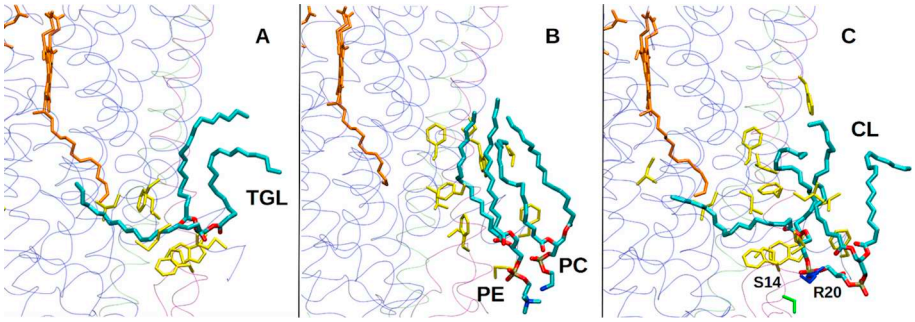

Fig. 6. Lipid binding site II. TGL (A), PC/PE (B) and CL (C) molecules bind to the site maintaining predominantly hydrophobic contacts. Basic, hydrophobic and polar residues in blue, yellow and green, respectively. Lipids are shown in stick representation with carbon, oxygen, nitrogen and phosphorus atoms in cyan, red, blue and brown, respectively. Hemes are displayed in orange licorice representation.

components are not modeled, the site is transiently occupied by different types of bulk lipids (Fig. 6B). Given the *cupped* shape of the site, it transiently traps lipid molecules, with interactions primarily hydrophobic in nature. In order to further test the binding of CL at this site, we replaced TGL molecule with a CL (setup 7) and performed a microsecond MD run. Similar to the tight binding of TGL, the CL molecule remained at the site, with predominantly hydrophobic interactions maintained with the protein (Fig. 6C) together with minor contributions from polar interactions to Arg20 and Ser14 of VIIc (chain L).

Earlier it was suggested that this site may participate in proton uptake via D channel [34]. Measurement of minimum distance between the D channel proton uptake site Asp91 (Cγ atom) and the nearest bound lipid head group shows this distance to be in the range of 15–25 Å (ca. 20 Å between TGL and D91 in the crystal structure), somewhat larger than the previous estimates [33]. Analysis of the region between site II lipids and Asp91 reveal that even though a number of conserved charged residues (Arg5, Asn11, Asp14) exist near the proton uptake site, a continuous hydrogen bond connectivity to site II lipid head group is in part blocked by a hydrophobic residue (Trp6) (Fig. 7). Instead, the tightly bound subunit III lipids are more likely to be important for rapid proton uptake through the D channel due to their shorter distance and direct effect on the pK_a of Asp91 [36]. We envisage that the primary role of TGL/CL at site II, which is stabilized by strong hydrophobic interactions, is to stabilize the *supercomplex* structure or its formation by making lipid (CL) mediated contacts with the ND5 subunit of complex I [37,38] (see Discussion).

3.5. CL assisted proton uptake through K channel

The presence of a negatively charged CL molecule next to proton uptake routes in respiratory complexes is often discussed [14,36]. In analogy to the presence of lipid head group next to the proton uptake site Asp91 [36], we find that CL molecules also stabilize next to the K proton channel (site IV, and see occupancy plots Figs. S3, S4, S6–S8). This site is buried between the two monomers and is therefore not accessible to bulk lipids. However, localization of CL molecules is observed in a number of monomeric oxidase simulations, suggesting our findings are statistically robust. We propose that this site (Fig. 8A)

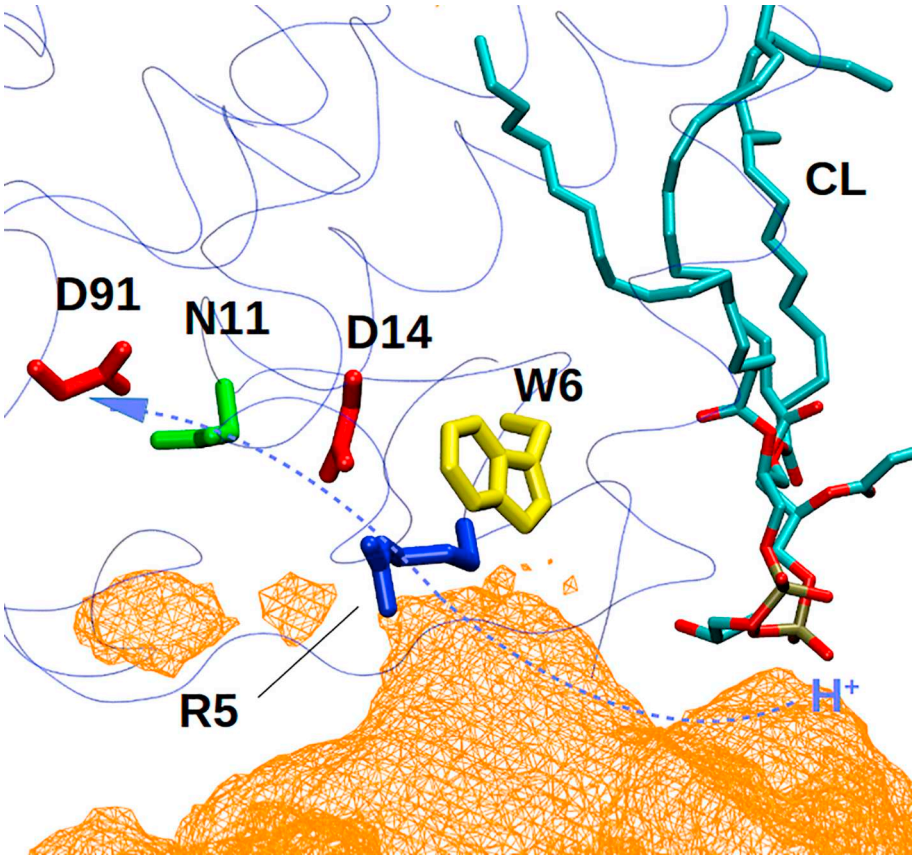

Fig. 7. Putative proton funneling path to Asp91 through bulk-water like conditions, where Trp6 forms a hydrophobic blockage between CL and Asp91. The water occupancy is shown at an isovalue of ca. 0.3 in orange mesh. Acidic, basic, hydrophobic and polar residues in red, blue, yellow and green, respectively. CL is shown in stick representation with carbon, oxygen and phosphorus atoms in cyan, red and brown, respectively.

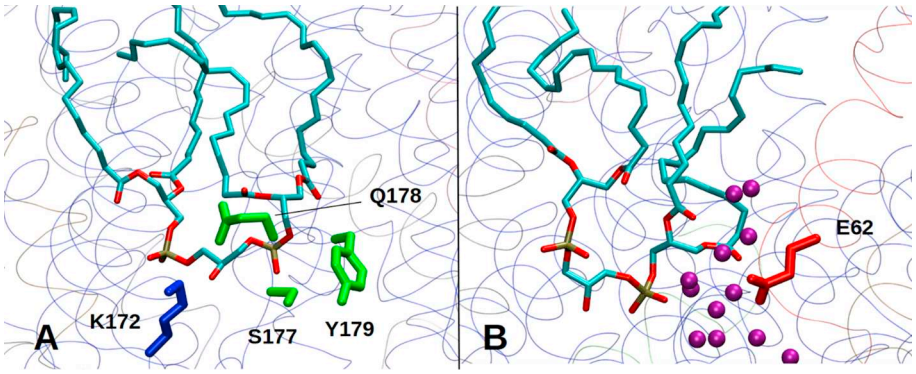

Fig. 8. (A) Polar interactions of CL bound at site IV. (B) Transient localization of CL next to proton uptake site E62 (subunit II) of K channel. Acidic, basic and polar residues in red, blue and green, respectively. CL is shown in stick representation with carbon, oxygen and phosphorus atoms in cyan, red and brown, respectively. Water molecules are displayed without hydrogens in magenta spheres in panel B.

represents one of the two weak CL binding sites observed in biochemical analysis [16], the other being CL1a/b.

Interestingly, the region adjacent to site IV is occupied by a cholate molecule in the crystal structure of bovine CcO, the carboxylate moiety of which forms a water-based connection to the putative proton uptake site Glu62 from subunit II. Indeed, a physiological role of small molecules binding at this location has been suggested based on X-ray data, biochemical and computational experiments [39]. We observe that a CL transiently (Figs. S3, S5 and S6) binds the site, mediating a water-based connection to Glu62 of subunit II (chain B) (see Fig. 8B). Such an interaction may play a role in rapid proton funneling towards the active site via Lys319/Glu62 pair of the K channel and also by altering the pK_a of Glu62 of subunit II (see Discussion).

4. Discussion

In this work atomistic simulations of dimeric and monomeric bovine C*c*O have been performed in the mitochondrial membrane like lipid bilayer. A number of novel findings emerge from these large-scale equilibrium molecular dynamics simulations of lipid-protein systems (Figs. S1 and S11). The simulation data show for the first time the dynamics of two crystallographically observed CL binding sites in C*c*O in full atomistic perspective. At one site, CL is loosely bound and dissociates rapidly, whereas on the other it is highly stabilized by charged-charged interactions. Removal of the latter CL creates massive lipid-protein conformational changes that would lead to loss of catalytic activity. Over longer timescales there will be a continuous exchange of protein bound CL molecules with the bulk lipids. For tight CL binding sites, where CL maintains strong charged-charged interactions with the protein, exchange will be a slow process. However, in the case of weak CL binding sites exchange will be faster, on the order of 1–10 μs, based on earlier coarse grained (CG) simulation estimates [33]. Even though similar statistics is not obtained in our short timescale atomistic simulations, which would be necessary to observe CL binding/unbinding events, the conclusion that CL binding sites between the two oxidase monomers are weak is also in agreement with the CL occupancy analysis from earlier CG simulation work [33].

Cardiolipin is a major component of the ETC and is important for a number of cellular processes [40]. CcO, the terminal respiratory enzyme, binds 3–4 CL molecules two of which are important for the full activity of the enzyme [15]. When these are removed using delipidation techniques, activity of the enzyme is reduced by 30–50% in detergent environment [16]. This means that the removal of CL molecules either affect the stability of the enzyme or affect the transport of electrons, protons or oxygen. The electron transfer path is distant from the lipid bilayer, and is buried in the shielding protein environment, so that it cannot be directly affected by its composition. Moreover, kinetic data show that the electron transfer reactions in oxidase are very fast (ns - μs) [1], and hence, are unlikely to be sufficiently perturbed by the changes in lipid composition, which are relatively slow. However, relatively slower diffusion of protons and oxygen from the outside to the active site may be affected by the bound lipid molecules. Importantly, our data show that the internal lipid binding sites (PG/PE molecules) and protein structure (subunits III and VIIa) next to the proton uptake site D91 (of D channel) are strongly affected upon removal of tightly bound crystallographic CL molecule at site I. These atomic level insights from our microsecond simulations are in strong alliance with earlier biochemical data, which show activity loss upon removal of tightly bound CLs [18]. We envisage that the perturbed architecture of lipid-protein site prevents rapid proton uptake through the D channel, which causes low catalytic activity due to suicide inactivation; a phenomenon displayed by the enzyme in the absence of subunit III or subunit III mutants [41]. Furthermore, the tails of the CL bound at this site brushes that of PG molecules buried in subunit III V-shaped cleft, which have been proposed to be important for oxygen delivery [11,36]. The perturbation caused by removing CL will also affect the transport of O_2 to the active site (see also [36]).

Interestingly, subunit III and its tightly bound lipids are found also in the bacterial A-type oxidases [1]. However, the binding and functional role of CL in bacterial enzyme remains unclear [42,43]. Sequence analysis reveal that only some of the charged residues that dynamically interact with CL (Tables 2, S1 and S2) are conserved (Arg221 and Lys224 of subunit III), suggesting that CL may not bind subunit III in bacterial oxidases at the same site as it does in bovine oxidase. However, it is possible that the similar role is played by other lipids specific to bacteria. Envisaging that the function of mitochondrial A type oxidases is much more tightly regulated than the bacterial counterparts [5], it remains possible that the tightly bound site I CL molecule provides enhanced stability to the mitochondrial enzyme.

A number of high resolution crystal structures of bovine CcO have been solved [44] in which it has been crystallized in its dimeric form stabilized by detergent-based environment. However, 2D crystals obtained in native-like membrane conditions reveal monomer form to be biologically relevant [45]. This is also supported by high resolution cryo electron microscopy structures of mitochondrial supercomplexes or *respirasomes* that show monomeric CcO to be aligned at the periphery of the membrane domain of complex I [38]. Though the data from our microseconds simulations do not reveal large scale perturbations in dimeric form of enzyme in membranous environment, but clearly shows weaker binding of CL buried between the two monomers. Thus, it is likely that in lipidic milieu both monomeric and dimeric populations of enzyme exist.

It is interesting to note that subunit VIIa which resides between the CL binding sites I and II, mediates interactions with other components of the respiratory chain (complexes I and III) in a respirasome [37,38]. It is possible that upon stringent delipidation of enzyme that removes also the tightly bound CLs at sites I and II, the resulting structural perturbation prevents the formation or cause destabilization of supercomplexes that comprise complex IV (see also [46]). Indeed, structural data on respirasomes display subunits III, VIIa, VIIc and VIII, that carry tight CL binding sites I and II, to be exposed to other components of respirasome.

In contrast to the supply of all pumped protons by the D channel in bacterial oxidases, the K channel transfers two protons to the active site in the reductive phase of the catalytic cycle. Interestingly, K channel has been suggested to be regulated by small molecules such as steroids [39], which may alter the activity of oxidase under variable physiological conditions, the mechanisms of which remains poorly understood. We find in our simulations occupancy of CL next to the proton uptake site of the K channel, Glu62 of subunit II. A transient CL binding at the site may enhance proton affinity of Glu62, similar to what has been suggested for the D channel proton uptake site Asp91 and lipids next to it [36]. Interestingly, experiments suggest functional takeover by small ligands that bind despite removal of Glu62 [39]. Considering a similar scenario, a CL may bind tightly in the absence of anionic Glu62 and play an important role in funneling protons to the active site via Lys319 of the K channel.

5. Conclusions

The terminal enzyme of the electron transport chain, cytochrome *c* oxidase, is central to energy metabolism in mitochondria. Despite detailed understanding of its mechanism, it remains unknown how it is regulated, and what roles lipids play in enzyme function. Here, we applied computational approach of molecular dynamics simulations to study the long-time behaviour of lipid-protein interactions. Based on microsecond simulation data we find that the cardiolipins that hold two monomers of oxidase together are weakly bound and dissociate rapidly without affecting the protein structure. In contrast, removal of second crystallographic cardiolipin molecule is found to be deleterious for the structure and function of enzyme. We highlight the strength of molecular dynamics simulation approaches, which are capable of describing events that otherwise are difficult to observe directly by current experimental techniques.

Supplementary data to this article can be found online at https://doi.org/10.1016/j.bbabio.2018.11.004.

Transparency document

The Transparency document associated with this article can be found, in online version.

Acknowledgements

We thank the Academy of Finland (294652), the University of Helsinki, the Sigrid Jusélius Foundation and the Magnus Ehrnrooth Foundation for financial support. The Center for Scientific Computing (CSC, Finland) is acknowledged for generous computational support. VS is thankful to Outi Haapanen for help with videos and Matti Javanainen, Professor Mårten Wikström and Professor Peter Rich for helpful discussions.

References

[1] M. Wikström, K. Krab, V. Sharma, Oxygen activation and energy conservation by cytochrome *c* oxidase, Chem. Rev. 118 (2018) 2469–2490.
[2] P.R. Rich, Mitochondrial cytochrome *c* oxidase: catalysis, coupling and controversies, Biochem. Soc. Trans. 45 (2017) 813–829.
[3] M.M. Pereira, M. Santana, M. Teixeira, A novel scenario for the evolution of haem–copper oxygen reductases, Biochimica et Biophysica Acta (BBA)-Bioenergetics 1505 (2001) 185–208.
[4] S. Shimada, K. Shinzawa-Itoh, J. Baba, S. Aoe, A. Shimada, E. Yamashita, J. Kang, M. Tateno, S. Yoshikawa, T. Tsukihara, Complex structure of cytochrome c–cytochrome c oxidase reveals a novel protein–protein interaction mode, EMBO J. 36 (2017) 291–300.
[5] V. Sharma, M. Wikström, A structural and functional perspective on the evolution of the heme–copper oxidases, FEBS Lett. 588 (2014) 3787–3792.
[6] P. Brzezinski, R.B. Gennis, Cytochrome *c* oxidase: exciting progress and remaining mysteries, J. Bioenerg. Biomembr. 40 (2008) 521–531.
[7] S. Supekar, A.P. Gamiz-Hernandez, V.R.I. Kaila, A protonated water cluster as a transient proton-loading site in cytochrome *c* oxidase, Angew. Chem. Int. Ed. 55 (2016) 11940–11944.
[8] V. Sharma, P.G. Jambrina, M. Kaukonen, E. Rosta, P.R. Rich, Insights into functions of the H channel of cytochrome *c* oxidase from atomistic molecular dynamics simulations, Proc. Natl. Acad. Sci. 201708628 (2017).
[9] C.Y. Son, A. Yethiraj, Q. Cui, Cavity hydration dynamics in cytochrome *c* oxidase and functional implications, Proc. Natl. Acad. Sci. 114 (2017) E8830–E8836.
[10] R. Liang, J.M. Swanson, M. Wikström, G.A. Voth, Understanding the essential proton-pumping kinetic gates and decoupling mutations in cytochrome *c* oxidase, Proc. Natl. Acad. Sci. 114 (2017) 5924–5929.
[11] K. Shinzawa-Itoh, H. Aoyama, K. Muramoto, H. Terada, T. Kurauchi, Y. Tadehara, A. Yamasaki, T. Sugimura, S. Kurono, K. Tsujimoto, T. Mizushima, E. Yamashita, T. Tsukihara, S. Yoshikawa, Structures and physiological roles of 13 integral lipids of bovine heart cytochrome ⟨em⟩c⟨/em⟩ oxidase, EMBO J. 26 (2007) 1713–1725.
[12] M. Schlame, J.A. Towbin, P.M. Heerdt, R. Jehle, S. DiMauro, T.J. Blanck, Deficiency of tetralinoleoyl-cardiolipin in Barth syndrome, Ann. Neurol. 51 (2002) 634–637.
[13] F. Valianpour, R.J. Wanders, P.G. Barth, H. Overmars, A.H. Van Gennip, Quantitative and compositional study of cardiolipin in platelets by electrospray ionization mass spectrometry: application for the identification of Barth syndrome patients, Clin. Chem. 48 (2002) 1390–1397.
[14] C. Hunte, Specific Protein–Lipid Interactions in Membrane Proteins, Portland Press Limited, 2005.
[15] N.C. Robinson, Functional binding of cardiolipin to cytochromec oxidase, J. Bioenerg. Biomembr. 25 (1993) 153–163.
[16] E. Sedlák, N.C. Robinson, Phospholipase A2 digestion of cardiolipin bound to bovine cytochrome *c* oxidase alters both activity and quaternary structure, Biochemistry 38 (1999) 14966–14972.
[17] E. Sedlák, R. Varhač, A. Musatov, N.C. Robinson, The kinetic stability of cytochrome *c* oxidase: effect of bound phospholipid and dimerization, Biophys. J. 107 (2014) 2941–2949.
[18] E. Sedlák, N.C. Robinson, Destabilization of the quaternary structure of bovine heart cytochrome *c* oxidase upon removal of tightly bound cardiolipin, Biochemistry 54 (2015) 5569–5577.
[19] J. Lee, X. Cheng, J.M. Swails, M.S. Yeom, P.K. Eastman, J.A. Lemkul, S. Wei, J. Buckner, J.C. Jeong, Y. Qi, CHARMM-GUI input generator for NAMD, GROMACS, AMBER, OpenMM, and CHARMM/OpenMM simulations using the CHARMM36 additive force field, J. Chem. Theory Comput. 12 (2015) 405–413.
[20] I. Liko, M.T. Degiacomi, S. Mohammed, S. Yoshikawa, C. Schmidt, C.V. Robinson, Dimer interface of bovine cytochrome *c* oxidase is influenced by local post-translational modifications and lipid binding, Proc. Natl. Acad. Sci. 113 (2016) 8230–8235.
[21] M.P. Johansson, V.R. Kaila, L. Laakkonen, Charge parameterization of the metal centers in cytochrome *c* oxidase, J. Comput. Chem. 29 (2008) 753–767.
[22] V. Sharma, G. Enkavi, I. Vattulainen, T. Róg, M. Wikström, Proton-coupled electron transfer and the role of water molecules in proton pumping by cytochrome *c* oxidase, Proc. Natl. Acad. Sci. 112 (2015) 2040–2045.
[23] J.B. Klauda, R.M. Venable, J.A. Freites, J.W. O'Connor, D.J. Tobias, C. Mondragon-Ramirez, I. Vorobyov, A.D. MacKerell Jr., R.W. Pastor, Update of the CHARMM all-atom additive force field for lipids: validation on six lipid types, J. Phys. Chem. B 114 (2010) 7830–7843.
[24] R.B. Best, X. Zhu, J. Shim, P.E. Lopes, J. Mittal, M. Feig, A.D. MacKerell Jr., Optimization of the additive CHARMM all-atom protein force field targeting improved sampling of the backbone ϕ, ψ and side-chain χ1 and χ2 dihedral angles, J. Chem. Theory Comput. 8 (2012) 3257–3273.
[25] A.D. MacKerell Jr., D. Bashford, M. Bellott, R.L. Dunbrack Jr., J.D. Evanseck, M.J. Field, S. Fischer, J. Gao, H. Guo, S. Ha, All-atom empirical potential for molecular modeling and dynamics studies of proteins, J. Phys. Chem. B 102 (1998) 3586–3616.
[26] H.J. Berendsen, J.V. Postma, W.F. van Gunsteren, A. DiNola, J. Haak, Molecular dynamics with coupling to an external bath, J. Chem. Phys. 81 (1984) 3684–3690.
[27] S. Nosé, A unified formulation of the constant temperature molecular dynamics methods, J. Chem. Phys. 81 (1984) 511–519.
[28] W.G. Hoover, Canonical dynamics: equilibrium phase-space distributions, Phys. Rev. A 31 (1985) 1695.
[29] M.J. Abraham, T. Murtola, R. Schulz, S. Páll, J.C. Smith, B. Hess, E. Lindahl, GROMACS: high performance molecular simulations through multi-level parallelism from laptops to supercomputers, SoftwareX 1 (2015) 19–25.
[30] B. Hess, P-LINCS: a parallel linear constraint solver for molecular simulation, J. Chem. Theory Comput. 4 (2008) 116–122.
[31] M. Parrinello, A. Rahman, Polymorphic transitions in single crystals: a new molecular dynamics method, J. Appl. Phys. 52 (1981) 7182–7190.
[32] W. Humphrey, A. Dalke, K. Schulten, VMD: visual molecular dynamics, J. Mol. Graph. 14 (1996) 33–38.
[33] C. Arnarez, S. Marrink, X. Periole, Identification of cardiolipin binding sites on cytochrome *c* oxidase at the entrance of proton channels, Sci. Rep. 3 (2013) 1263.
[34] E. Sedlák, M. Panda, M.P. Dale, S.T. Weintraub, N.C. Robinson, Photolabeling of cardiolipin binding subunits within bovine heart cytochrome *c* oxidase, Biochemistry 45 (2006) 746–754.
[35] K. Gupta, J.A. Donlan, J.T. Hopper, P. Uzdavinys, M. Landreh, W.B. Struwe, D. Drew, A.J. Baldwin, P.J. Stansfeld, C.V. Robinson, The role of interfacial lipids in stabilizing membrane protein oligomers, Nature 541 (2017) 421.
[36] V. Sharma, P. Ala-Vannesluoma, I. Vattulainen, M. Wikström, T. Róg, Role of subunit III and its lipids in the molecular mechanism of cytochrome *c* oxidase, Biochimica et Biophysica Acta (BBA)-Bioenergetics 1847 (2015) 690–697.
[37] K.M. Davies, T.B. Blum, W. Kühlbrandt, Conserved in situ arrangement of complex I and III2 in mitochondrial respiratory chain supercomplexes of mammals, yeast, and plants, Proc. Natl. Acad. Sci. 115 (2018) 3024–3029.
[38] D. Milenkovic, J.N. Blaza, N.-G. Larsson, J. Hirst, The enigma of the respiratory

chain supercomplex, Cell Metab. 25 (2017) 765–776.
[39] C. Hiser, J. Liu, S. Ferguson-Miller, The K-path entrance in cytochrome *c* oxidase is defined by mutation of E101 and controlled by an adjacent ligand binding domain, Biochimica et Biophysica Acta (BBA)-Bioenergetics 1859 (2018) 725–733.
[40] G. Paradies, V. Paradies, V. De Benedictis, F.M. Ruggiero, G. Petrosillo, Functional role of cardiolipin in mitochondrial bioenergetics, Biochimica et Biophysica Acta (BBA)-Bioenergetics 1837 (2014) 408–417.
[41] L. Varanasi, D. Mills, A. Murphree, J. Gray, C. Purser, R. Baker, J. Hosler, Altering conserved lipid binding sites in cytochrome *c* oxidase of Rhodobacter sphaeroides perturbs the interaction between subunits I and III and promotes suicide inactivation of the enzyme, Biochemistry 45 (2006) 14896–14907.
[42] X. Zhang, B. Tamot, C. Hiser, G.E. Reid, C. Benning, S. Ferguson-Miller, Cardiolipin deficiency in Rhodobacter sphaeroides alters the lipid profile of membranes and of crystallized cytochrome oxidase, but structure and function are maintained, Biochemistry 50 (2011) 3879–3890.
[43] K.S. Alnajjar, T. Cvetkov, L. Prochaska, Role of phospholipids of subunit III in the regulation of structural rearrangements in cytochrome *c* oxidase of Rhodobacter sphaeroides, Biochemistry 54 (2015) 1053–1063.
[44] S. Yoshikawa, A. Shimada, Reaction mechanism of cytochrome *c* oxidase, Chem. Rev. 115 (2015) 1936–1989.
[45] Y. Osuda, K. Shinzawa-Itoh, K. Tani, S. Maeda, S. Yoshikawa, T. Tsukihara, C. Gerle, Two-dimensional crystallization of monomeric bovine cytochrome *c* oxidase with bound cytochrome *c* in reconstituted lipid membranes, J. Electron Microsc. 65 (2016) 263–267.
[46] S. Bazán, E. Mileykovskaya, V.K. Mallampalli, P. Heacock, G.C. Sparagna, W. Dowhan, Cardiolipin-dependent reconstitution of respiratory supercomplexes from purified *Saccharomyces cerevisiae* complexes III and IV, J. Biol. Chem. M112 (425876) (2012) jbc.